X-ray reflectivity and diffuse scattering

A. Gibaud* and S. Hazra

Université du Maine, Faculté des Sciences, UPRES-A 6087, 72085 Le Mans, Cedex 9, France

X-ray specular reflectivity and diffuse scattering techniques are presented and illustrated with experimental results obtained on different kinds of thin films and surfaces. After a short introduction on the Fresnel reflectivity, the matrix technique is developed; the kinematical Born approximation is then deduced from the dynamical theory. In this approximation it is shown how the diffuse scattering contribution can be analysed.

1. Introduction

X-ray reflectivity has become an invaluable tool to study the structure and the organization of materials which are grown as thin films at the submicronic and atomic scales[1–6]. In thin film material research, the trend is to design solid films of increasing complexity having specific properties for technical applications. The nature of the materials deposited on substrates and the techniques of deposition for such applications are extremely variable. The design of semiconductor and metallic heterostructures is well mastered by molecular beam epitaxy deposition which generally provides extremely well-crystallized materials. This technique which is expensive is used in general for making specific materials such as quantum wells and artificial superlattices. Less expensive techniques are now developed and beautiful examples of supramolecular structures can now be achieved by assembling molecules of different kinds at the surface of a substrate[7]. Well-organized structures made in such a way can provide electronic analogues, electrochromic or nonlinear optical elements. Such multilayer architectures can be achieved by the LB method and by self-assembly of the layers through covalent bonds or metal coordination. For industrial applications the sputtering technique is also widely used for coating metallic films, for making oxide thin films and for creating heterogeneous materials like cermets (ceramic metals). As can be seen there are many ways to create complex mesoscopic layered structures which in turn will be considered as interesting if their structure appears to be as perfect as possible.

The perfection of mesoscopic layered super-structures is defined both by the quality of the interfaces and by the reproducibility with which one can achieve the deposition of the layers (control of thickness, crystallinity, voids or various defects which may appear during the growth process). In particular, the roughness of the interfaces is of crucial importance for many technological applications and it is a parameter which must be determined to appreciate the quality of the interfaces.

In this paper, we shall present the technique of specular X-ray reflectivity and show through various examples how it can be used to determine the electron density profile (EDP) and the roughness of the interfaces. The measurement of diffuse X-ray scattering will be presented as a good way to analyse the correlation of interfacial roughness between successive layers. We will also discuss briefly the method of studying the morphology of heterogeneous thin films by means of X-ray scattering.

2. Basic principles of X-ray reflectivity

2.1. *The index of refraction*

X-rays are part of the broad spectrum of electromagnetic waves. X-rays can be produced by the acceleration or deceleration of electrons either in vacuum (synchrotrons) or in metallic targets (tubes). The most widely used X-rays in materials science have a typical wavelength, λ, of the order of 0.1 nm. This wavelength is associated with a very high frequency of the order of 10^{19} Hz which is at least four orders of magnitude greater than the eigen frequency of an electron bound to a nucleus. As a consequence, the interaction of X-rays with matter can be well described (in a classical way for a first approach) by an index of refraction which characterizes the change of direction of the X-ray beam when passing from air to a material. A very simple classical model in which an electron of the material is considered to be accelerated by the X-ray field shows that the index of refraction for X-rays can be written as

$$n = 1 - \delta - i\beta,$$

where δ and β account for the scattering and absorption of the material, respectively. The sign preceding β depends on the convention of signs used to define the propagation of the electric field. The values of δ and β (which are positive) depend on the electron density, ρ, and linear absoption coefficient, μ, of the material through the following relations

*For correspondence. (e-mail: Alain.Gibaud@univ-lemans.fr)

$$n = 1 - \sum_k \frac{Z_k + f_k' + if_k''}{V_m},$$

where

$$\delta = \frac{r_e}{2\pi}\lambda^2 \sum_k \frac{(Z_k + f_k')}{V_m} = \frac{r_e}{2\pi}\lambda^2 \rho,$$

and

$$\beta = \frac{r_e}{2\pi}\lambda^2 \sum_k \frac{f''}{V_m} = \frac{\lambda}{4\pi}\mu,$$

where $r_e = 2.813 \times 10^{-6}$ nm is the classical radius of the electron, V_m is the volume of the unit cell, Z_k is the number of electrons of atom k in the unit cell, f' and f'' are the real and imaginary parts of the absorption for the specific energy of the incident radiation λ. The sum is performed over all the atoms of the unit cell.

2.2. *The critical angle of reflection*

For X-rays, the refractive index of a material is slightly less than unity[8]. Passing from air ($n = 1$) to the reflecting material ($n < 1$), it is possible to totally reflect the beam if the incident angle θ (which is the angle between the surface of the sample and the incident beam) is small enough. This is known as the *total external reflection* of X-rays. For this to occur, the incident angle must be smaller than the critical angle θ_c defined as

$$\cos\theta_c = n = 1 - \delta.$$

Since n is very close to unity, this angle is very small and a Taylor approximation in θ_c yields

$$\theta_c^2 = 2\delta = \frac{r_e\lambda^2}{\pi}\rho.$$

2.3. *Reflected intensity from ideally flat surface*

When an X-ray beam impinges on a flat material, part of the incoming intensity is reflected and part of it is transmitted through the material. If the surface of the reflecting material is flat, the reflected intensity will be confined in a direction symmetric from the incident one and will be labelled as *specular*. The specular reflectivity is conventionally defined as the ratio

$$R(\theta) = \frac{I(\theta)}{I_0},$$

where $I(\theta)$ is the reflected intensity at angle θ and I_0 is the intensity of the incident beam. The domain of validity of X-ray reflectivity is limited to small angles of incidence where it is possible to consider the electron density as continuous. In this approximation, the reflection can be treated as a classical problem of reflection of an electromagnetic wave at an interface. The reflected amplitude is obtained by writing the continuity of the electric field and of the magnetic field at the interface. This leads to the classical Fresnel relationship which gives the reflection coefficient in amplitude for the (s) and (p) polarization. The reflectivity which is the modulus square of this coefficient can be formulated in the case of X-rays as

$$R^{flat}(\theta) = rr^* = \left|\frac{\theta - \sqrt{\theta^2 - \theta_c^2 - 2i\beta}}{\theta + \sqrt{\theta^2 - \theta_c^2 - 2i\beta}}\right|^2.$$

This expression is independent of the polarization. Since the reflectivity is only observed in specular conditions (incident angle equal to the exit angle), we obtain after introduction of the wave vector transfer $\vec{q} = (0, 0, q_z = 4\pi \sin\theta/\lambda)$

$$R^{flat}(q_z) = \left|\frac{q_z - \sqrt{q_z^2 - q_c^2 - \frac{32i\pi^2\beta}{\lambda^2}}}{q_z + \sqrt{q_z^2 - q_c^2 - \frac{32i\pi^2\beta}{\lambda^2}}}\right|^2.$$

Figure 1 shows the reflectivity of a silicon wafer calculated using this formula and using a power law formula which is valid when $q_z > 3q_c$. The deviation from unity at low q_z is due to the absorption in

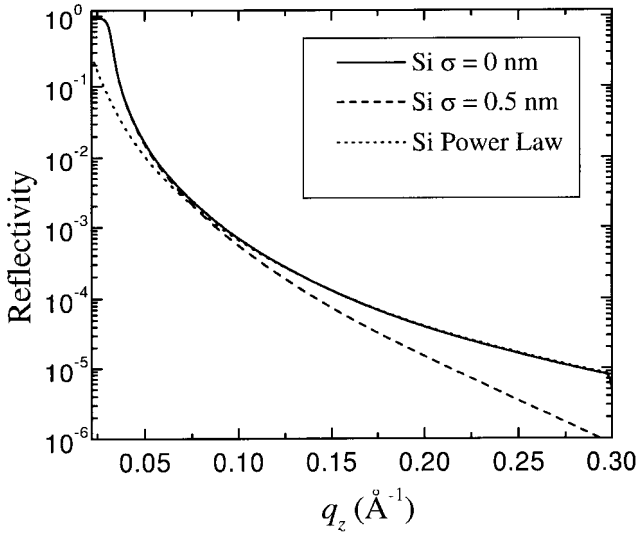

Figure 1. X-ray reflectivity from a silicon wafer for no surface roughness, for a roughness $\sigma = 0.5$ nm and in the power law regime. One can see that the roughness plays a major role at high wave vector transfers and that the power law regime differs from the Fresnel reflectivity at low wave vector transfers.

the material which plays a major role close to $q = q_c = 4\pi\theta_c/\lambda$.

2.4. *Importance of surface roughness*

Ideal flat surfaces are fictitious especially when they are analysed with X-rays or neutron reflectometry. Such techniques are indeed extremely sensitive to any defects of flatness. It is easy to realize that rough surfaces will be less reflecting than an ideally flat surface. It is thus important to describe the effect of roughness on the measured reflected intensity. The *roughness*, σ, of the surface can be apprehended statistically with the help of the moments of the distribution, $P(z)$, and of altitude $z(x, y)$ with respect to the mean altitude $\bar{z}$ by the following relation

$$\sigma^2 = \langle (z(x, y) - \bar{z}^2 \rangle = \int P(z)(z(x, y) - \bar{z})^2 \mathrm{d}z.$$

It is usual to introduce a height difference correlation function $g(X, Y)$ which correlates the two heights $z(x, y)$ and $z(x' = x + X, y' = y + Y)$ on the surface as

$$g(X, Y) = \langle (z(x, y) - z(x', y'))^2 \rangle$$
$$= \langle z^2(x, y) \rangle + \langle z^2(x', y') \rangle - 2\langle z(x, y)z(x', y') \rangle,$$

where the averaging is taken over the area coherently illuminated by the beam. We assume the surface to present the property of stationarity, i.e. the mean value of the square of the altitude does not depend on the position, so that $\langle z^2(x, y) \rangle = \langle z^2(x', y') \rangle = \sigma^2$. As a result

$$g(X, Y) = 2\sigma^2 - 2\langle z(x, y)z(x', y') \rangle = 2\sigma^2 - 2C(X, Y),$$

where $C(X, Y)$ is the *height–height correlation function* defined as

$$C(X, Y) = \frac{1}{L_x}\frac{1}{L_y}\int_{-\frac{L_y}{2}}^{\frac{L_y}{2}}\int_{-\frac{L_x}{2}}^{\frac{L_x}{2}} z(x, y)z(y + Y, x + X)\mathrm{d}x\mathrm{d}y.$$

As shown in Figure 1, the effect of surface roughness is to reduce the specular reflectivity by a kind of Debye–Waller factor (this will be evidenced later on). When the correlation length of the height fluctuations is not very large then $R^{rough}(q_z) = R^{flat}(q_z)e^{-q_{z,0}q_{z,1}\sigma^2}$ (where $q_{z,0}$ and $q_{z,1}$ are the wave vector transfers in air and in the material) and for large q_z this may be simplified as $R^{rough}(q_z) = R^{flat}(q_z)e^{-q_{z,0}^2\sigma^2}$ (refs 9 and 10). A similar effect is produced by a flat graded layer in which the electron density is represented by an error function of half width σ.

2. 5. *X-ray reflection by planar multilayers with flat and rough interfaces*

When the wave propagates in a heterogeneous medium presenting regions of different electron densities, it is not possible to directly use the Fresnel coefficients. The calculation is performed by applying the boundary conditions of the electric and magnetic fields at each interface[11–13]. The fact that multiple reflections are taken into account in the calculation leads to the *dynamical theory* of reflection and the result is usually presented as the product of matrices. For this, let us consider a plane wave polarized in the direction perpendicular to the plane of incidence(s) and propagating in the medium j of a stratified material and let us choose the axes so that the wave is travelling in the xz plane (Figure 2). For the electric field in medium j, solution of the Helmoltz's equation, is

$$E_j(x, z) = (A_j^+ e^{ik_{zj}z} + A_j^- e^{-ik_{zj}z})e^{i(\omega t - k_{xj}x)}$$
$$= (U_j^+(z) + U_j^-(z))e^{i(\omega t - k_{xj}x)},$$

where $k_{z,j}$ (resp. $k_{x,j}$) is the z (resp. x) component of the wave vector in medium j. It can be shown that $k_{z,j} = k_j \sin\theta_j = k\sqrt{\theta^2 - 2\delta_j - 2i\beta_j}$. The condition of continuity of the tangential component of the electric and magnetic fields and the conservation of $k_{x,j}$ at interface j, $j + 1$ located at $z = z_{j+1}$ yield

$$U_j^+(z_{j+1}) + U_j^-(z_{j+1}) = U_{j+1}^+(z_{j+1}) + U_{j+1}^-(z_{j+1}),$$
$$k_{z,j}[U_j^+(z_{j+1}) - U_j^-(z_{j+1})] = k_{z,j+1}[U_{j+1}^+(z_{j+1}) - U_{j+1}^-(z_{j+1})].$$

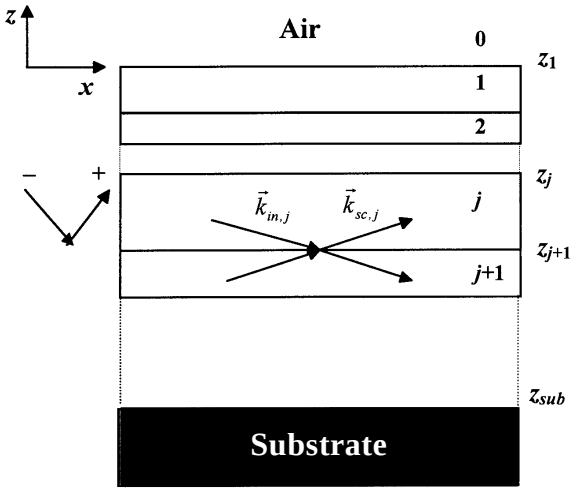

Figure 2. Schematic of a layered material and the conventions used in the text concerning the labels of the layers and of the propagation directions of the incident and reflected waves. (Note that the first air–material interface begins at altitude z_1.)

These two equations can be combined in a matrix form yielding

$$\begin{bmatrix} U_j^+(z_{j+1}) \\ U_j^-(z_{j+1}) \end{bmatrix} = \begin{bmatrix} p_{j,j+1} & m_{j,j+1} \\ m_{j,j+1} & p_{j,j+1} \end{bmatrix} \begin{bmatrix} U_{j+1}^+(z_{j+1}) \\ U_{j+1}^-(z_{j+1}) \end{bmatrix},$$

with

$$p_{j,j+1} = \frac{k_{z,j} + k_{z,j+1}}{2k_{z,j}},\ m_{j,j+1} = \frac{k_{z,j} - k_{z,j+1}}{2k_{z,j}}.$$

The matrix which transforms the amplitudes of the electric field from medium j to medium $j + 1$ will be denoted by the refraction matrix $\mathbf{R}_{j,j+1}$. In addition, in medium j, the amplitude of the electric field varies with altitude h as follows

$$\begin{bmatrix} U_j^+(z) \\ U_j^-(z) \end{bmatrix} = \begin{bmatrix} e^{-ik_{z,j}h} & 0 \\ 0 & e^{ik_{z,j}h} \end{bmatrix} \begin{bmatrix} U_j^+(z+h) \\ U_j^-(z+h) \end{bmatrix}.$$

The transfer matrix which is involved here will be denoted by the translation matrix $\mathbf{T}_j$. The amplitude of the electric field at the surface (altitude $z_1 = 0$) of the layered material is obtained by multiplying all the refraction and translation matrices in each layer starting from the substrate (at z_{sub}) as follows

$$\begin{bmatrix} U_0^+(z_1) \\ U_0^-(z_1) \end{bmatrix} = \mathbf{R_{0,1}T_1R_{1,2}}\ldots\ldots\ldots\mathbf{R_{sub-1,sub}} \begin{bmatrix} U_{sub}^+(z_{sub}) \\ U_{sub}^-(z_{sub}) \end{bmatrix} = \begin{bmatrix} M_{11} & M_{12} \\ M_{21} & M_{22} \end{bmatrix} \begin{bmatrix} U_{sub}^+(z_{sub}) \\ U_{sub}^-(z_{Sub}) \end{bmatrix}.$$

The product of all these matrices is a 2×2 matrix called the transfer matrix $\mathbf{M}$. The coefficient of reflection in amplitude of the electric field at the surface of the material is given by

$$r = \frac{U_0^+(z_1)}{U_0^-(z_1)} = \frac{M_{11}U_{sub}^+(z_{sub}) + M_{12}U_{sub}^-(z_{sub})}{M_{12}U_{sub}^+(z_{sub}) + M_{22}U_{sub}^-(z_{sub})}.$$

As X-rays penetrate only over a few microns, it is legitimate to assume that no wave comes back from the substrate so that $U_{sub}^+(z_{sub}) = 0$ and

$$r = \frac{M_{12}}{M_{22}}.$$

This method known as the matrix technique is general and is valid for any kind of electromagnetic wave. The above formalism can be extended to slabs presenting uncorrelated rough interfaces. For this, one can show that the coefficient $m_{j,j+1}$ for flat interface has to be multiplied by $e^{-q_{z,j}q_{z,j+1}\sigma_{j+1}^2/2}$ to get coefficients for a rough interface.

We now present some examples of the usefulness of the matrix technique starting with a flat homogeneous material (1 layer system) for which the transfer matrix is $\mathbf{R_{0,1}}$ and

$$r^{flat} = r_{0,1} = \frac{m_{0,1}}{p_{0,1}} = \frac{k_{z,0} - k_{z,1}}{k_{z,0} + k_{z,1}} = \frac{\theta - \sqrt{\theta^2 - 2\delta - 2i\beta}}{\theta + \sqrt{\theta^2 - 2\delta - 2i\beta}},$$

i.e.

$$R^{flat} = \left| \frac{\theta - \sqrt{\theta^2 - 2\delta - 2i\beta}}{\theta + \sqrt{\theta^2 - 2\delta - 2i\beta}} \right|^2.$$

One can see by this example that the matrix technique gives the same expression as the Fresnel formulae.

For a single layer on a substrate (2 layers system), the transfer matrix is $\mathbf{R_{0,1}T_1R_{1,2}}$ and the reflection coefficient yields

$$r^{flat} = \frac{m_{0,1}p_{1,2}e^{ik_{z,1}h} + p_{0,1}m_{1,2}e^{-ik_{z,1}h}}{m_{0,1}m_{1,2}e^{ik_{z,1}h} + p_{0,1}p_{1,2}e^{-ik_{z,1}h}}.$$

Introducing the reflection coefficients $r_{j,j+1} = m_{j,j+1}/p_{j,j+1}$ at the interface j, $j + 1$, we get

$$r^{flat} = \frac{r_{0,1} + r_{1,2}e^{-2ik_{z,1}h}}{1 + r_{0,1}r_{1,2}e^{-2ik_{z,1}h}}.$$

It is worth noting that the denominator of this expression differs from unity by a term which corresponds to *multiple reflections* in the material as evidenced by the product of the two reflection coefficients $r_{0,1}r_{1,2}$. The reflected intensity is therefore

$$R^{flat} = \frac{r_{0,1}^2 + r_{1,2}^2 + 2r_{0,1}r_{1,2}\cos 2k_{z,1}h}{1 + r_{0,1}^2r_{1,2}^2 + 2r_{0,1}r_{1,2}\cos 2k_{z,1}h}.$$

The existence of cosine terms in the reflectivity clearly indicates that the reflectivity does present periodic oscillations in reciprocal space defined as

$$2k_{z,1}h = q_{z,1}h = 2p\pi.$$

The oscillations are the result of constructive interference between the reflected waves at interfaces 1 and 2 and their period gives the thickness of the film. Figure 3 corresponding to the reflectivity of diblock copolymer deposited on silicon is a good illustration of observable

interference. The fact that the reflectivity is less than 1 below the critical angle is related to a surface effect. At very shallow angles, it frequently happens that the footprint of the beam is larger than the sample surface so that only part of the intensity is reflected. A correction must then be applied to describe this part of the reflectivity curve[14]. Figure 4 shows the influence of surface and interface roughness on the reflectivity of a gold thin film deposited on a silicon substrate. Here σ_0 and σ_1 represent roughness at film surface and film/substrate interface, respectively.

For two layers deposited on a substrate the analytical expression of the reflectivity becomes tedious. The case

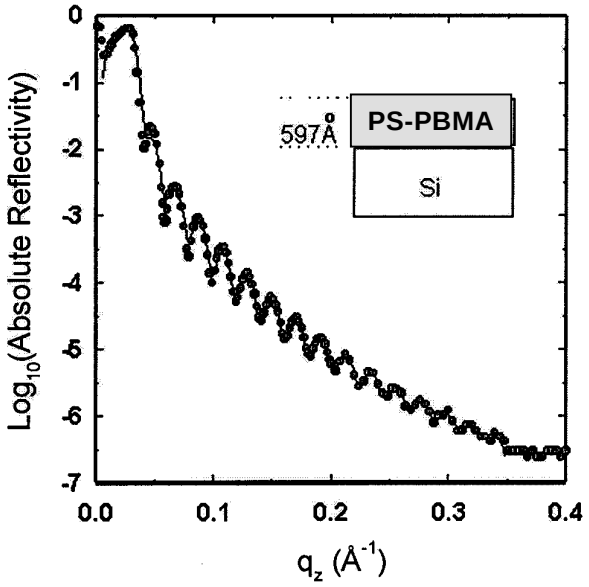

Figure 3. X-ray reflectivity from a homogeneous thin film of PS-PBMA (polystyrene-polybutyl-methacrylate) deposited on a silicon wafer.

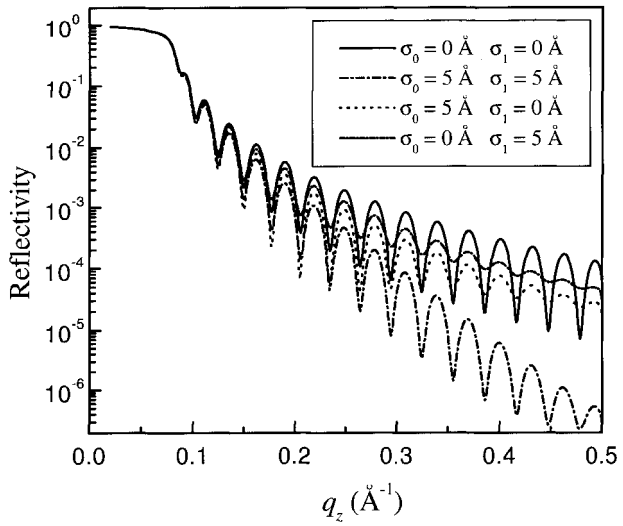

Figure 4. Influence of surface and interface roughness on the reflectivity of a thin film of gold deposited on a silicon substrate.

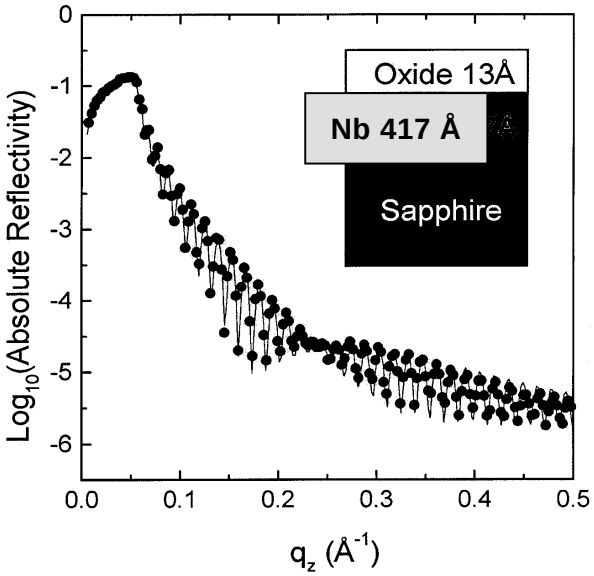

Figure 5. X-ray reflectivity of a Nb thin film deposited by MBE on a sapphire substrate. The attenuation of the short period oscillations is due to the presence of a thin layer of niobium oxide.

of a niobium thin film deposited on a sapphire substrate[15] is shown in Figure 5. Due to the oxidation of Nb, the oxide slowly grows as a function of time and levels off around 1.5 nm after a few hours of exposure in air. The reflectivity displays a typical shape with rapid oscillations due to the niobium layer, and a beating due to the presence of two interfaces at nearly the same altitude from the silicon surface.

The reflectivity curve of a multilayer exhibits a typical shape in which one can find Bragg peaks separated by Kiessig fringes[15–17]. The distance in q space between two Bragg peaks is inversely proportional to the period of the multilayer and the one between Kiessig fringes gives the thickness of the film (one should expect $N - 2$ fringes between two Bragg peaks, N being the number of repeated bilayers). Figure 6 shows a reflectivity curve of a 6-bilayer Cd-stearate LB film deposited on hydrophobic Si substrate. The EDP obtained from the fitting of the reflectivity curve is shown as an inset in the figure, which gives the total film thickness; location of Cd ions, their diffusion and separation, and also the packing of the film.

3. Dynamical to kinematical theory

The dynamical theory rigorously describes the specular reflectivity of flat surfaces but it is difficult to use the theory in the case of rough surfaces where a non-negligible part of the intensity is scattered off-specular. With some approximations, it is possible to derive the kinematical theory which is more flexible to use. The necessary approximation is known as the *Born approxi-*

mation. We describe in this section the different approximations which lead to the Born approximation by following the work of Hamley and Pedersen[18]. The dynamical expression for the reflected amplitude from a thin film of thickness h, can easily be extended to a large number of layers if we neglect multiple reflections. When the refraction is also neglected in the phase shift then this yields

$$r = \sum_{j=1}^{n} r_{j,j+1} e^{iq_z \sum_{m=0}^{j-1} d_m},$$

which can be expressed as

$$r = 4\pi r_e \sum_{j=1}^{n} \frac{(\rho_{j+1} - \rho_j)}{q_z^2} e^{iq_z \sum_{m=0}^{j-1} d_m}.$$

If we choose the origin of altitudes at the surface of the substrate (medium 0 at altitude $z_1 = 0$), we can replace in the phase factor, the sum over d_m by the altitude z_{j+1} of the interface j, $j + 1$ and thus

$$r = 4\pi r_e \sum_{j=1}^{n} \frac{(\rho_{j+1} - \rho_j)}{q_z^2} e^{iq_z z_{j+1}}.$$

If we consider that the material is made up of an infinite number of thin layers, the sum is transformed into an integral over z, and r becomes

$$r = \frac{4\pi r_e}{q_z^2} \int_{-\infty}^{+\infty} \frac{d\rho(z)}{dz} e^{iq_z z} dz.$$

The introduction of the Fresnel reflectivity of the substrate, $R_F(q_z) = (4\pi r_e \rho_s)^2/q_z^4$, in the above expression shows that in the first Born approximation the reflectivity can be written as

$$R(q_z) = rr^* = R_F(q_z) \left| \frac{1}{\rho_s} \int_{-\infty}^{+\infty} \frac{d\rho(z)}{dz} e^{iq_z z} dz \right|^2.$$

The above expression of $R(q_z)$ is not rigorous but can be easily handled in analytical calculations and is widely used among the polymer community[19,20]. In addition, if we follow the Wiener–Kintchine theorem we have

$$\frac{R(q_z)}{R_F(q_z)} = TF[\rho'(z) \otimes \rho'(z)],$$

so that the data inversion gives the autocorrelation function of the first derivative of the electron density. As shown in Figure 7, the data inversion immediately produces the thickness of the layers and has been successfully tested in several cases[21,22]. The width of the peaks depends on the roughness of the interfaces and their height on the difference in electron densities.

These approximations are also ideal to introduce another formulation of the reflected intensity. Using the relation between the Fourier transform of a function and that of its first derivative, one can write

$$R(q_z) = \frac{(4\pi r_e)^2}{q_z^2} \left| \int_{-\infty}^{+\infty} \rho(z) e^{iq_z z} dz \right|^2 = \frac{(4\pi r_e)^2}{q_z^2} \iint \rho(z)\rho(z') e^{iq_z(z-z')} dz dz'.$$

This expression is well-known in the Born approximation of X-ray diffraction or the so-called *kinematical theory*. It is valid for a plane wave and in the case of diffraction at an infinite distance from the sample to the source or to the detector (Fraunhofer approximation). This means that we do not consider here the effect of the resolution of the instrument.

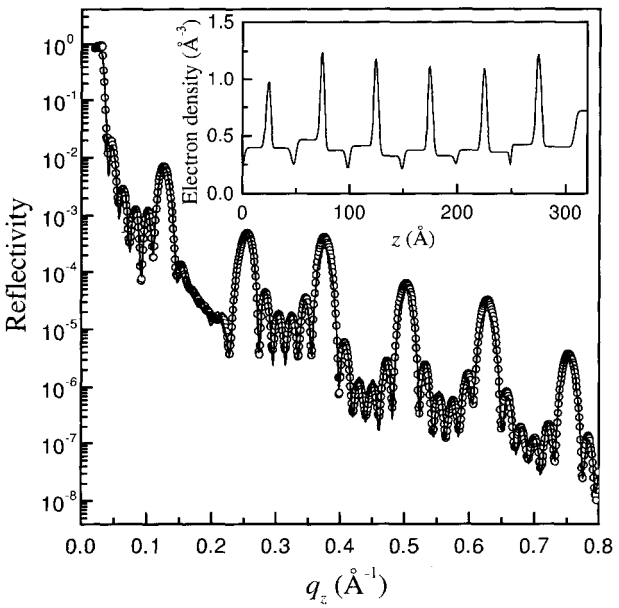

Figure 6. X-ray reflectivity of 6 bilayers of Cd-stearate LB film deposited on a silicon substrate. Inset shows the EDP obtained for the best fit curve.

4. Diffuse scattering

4.1. *Scattering cross-section within the Born approximation*

In the Born approximation[23,24] where the multiple reflections are neglected, the scattering cross-section is

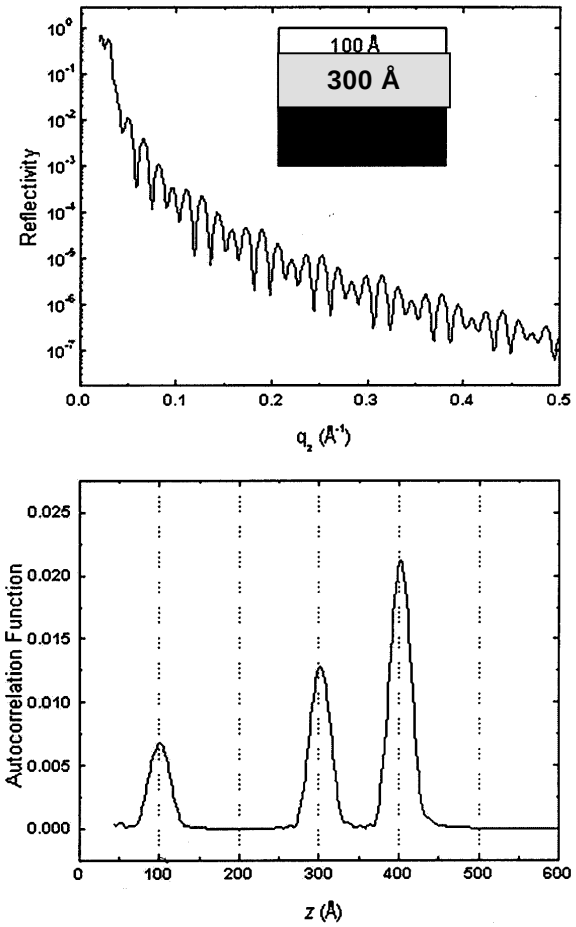

Figure 7. X-ray reflectivity of a system of two layers deposited on a silicon substrate together with the data inversion which clearly shows the presence of peaks in the autocorrelation function corresponding to the thickness of the layers.

the Fourier transform of the density–density autocorrelation function and is defined as

$$S(\vec{q}) = r_e^2 \iint \rho(\vec{r})\rho(\vec{r}\,')r^{i\vec{q}.(\vec{r}-\vec{r}\,')}\mathrm{d}r\mathrm{d}r'.$$

At small angles, X-rays are only sensitive to the mean electron density which is a constant if the material is homogeneous. In the above equation, the phase factor defines the phase shift between the waves scattered by the two points r and r' when one looks at the position q in reciprocal space. It is possible to show that when the integration along the z direction is performed from $-\infty$ to $z(X, Y)$, the scattering cross-section yields

$$S(\vec{q}) = \frac{\rho^2 r_e^2 L_x L_y}{q_z^2} \iint_S e^{-\frac{q_z^2}{2}\langle (z(X,Y)-z(0,0))^2\rangle} e^{i(q_x X + q_y Y)}\mathrm{d}X\mathrm{d}Y.$$

We thus observe that the scattering cross-section depends on the function $g(R)$ defined in section 2.4 and becomes

$$S(\vec{q}) = \frac{\rho_{el}^2 r_e^2 L_x L_y}{q_z^2} \iint_S e^{-\frac{q_z^2}{2}g(R)} e^{i(q_x.X + q_y.Y)}\mathrm{d}X\mathrm{d}Y.$$

This leads to

$$S(\vec{q}) = \frac{\rho_{el}^2 r_e^2 L_x L_y}{q_z^2} e^{-q_z^2\sigma^2} \iint_S e^{q_z^2 C(R)} e^{i(q_x.X + q_y.Y)}\mathrm{d}X\mathrm{d}Y.$$

For non-periodic surfaces, the height–height correlation function generally steadily decreases and the use of a stretched exponential to describe the decrease is frequent. Sinha *et al.*[23] have used for isotropic surfaces the following functional form

$$C(R) = \sigma^2 e^{-(R/\xi)^{2h}}.$$

The roughness exponent h is the key parameter which describes the height fluctuations at the surface: small h values produce very rough surfaces while if h is close to 1 the surface is more regular. The roughness σ governs the amplitude of the fluctuations and the parameter ξ is the correlation length of the height fluctuations. We can also note that the above correlation function is not universal. For liquids and surfaces close to the roughening transitions other functional forms are used[25,26].

4.2. *Ideally flat surfaces*

For ideally flat surfaces $g(R)$ is zero everywhere at the surface and the scattering cross-section yields

$$S(\vec{q}) = \frac{\rho_{el}^2 r_e^2 L_x L_y}{q_z^2} \iint_S e^{i(q_x X + q_y Y)}\mathrm{d}X\mathrm{d}Y.$$

The integral is the Fourier transform of a constant so that

$$S(\vec{q}) = \frac{4\pi^2 \rho_{el}^2 r_e^2 L_x L_y}{q_z^2} \delta q_x \delta q_y,$$

leading to the following well-known reflectivity

$$R(\vec{q}) = \frac{16\pi^2 r_e^2 \rho_{el}^2}{q_z^4}.$$

The reflectivity decreases as a power law with q_z and is defined by Dirac distributions in the orthogonal directions. Thus showing that for a flat surface the reflectivity is strictly *specular*.

4.3. *Rough surfaces without cut-off*

We now consider self-affine rough surfaces presenting a correlation length large in comparison with the coherence length with the beam at the surface. As previously reported $g(R)$ is given by

$$g(R) = 2\sigma^2(1 - e^{-(R/\xi)^{2h}}),$$

and if $R/\xi << 1$,

$$g(R) = 2\sigma^2\left(\frac{R}{\xi}\right)^{2h}.$$

This function can be written as

$$g(R) = \frac{2\sigma^2}{\xi^{2h}} R^{2h} = AR^{2h}.$$

The scattering cross-section yields

$$S(\vec{q}) = \frac{\rho_{el}^2 r_e^2 L_x L_y}{q_z^2} \iint_S e^{-\frac{q_z^2}{2} AR^{2h}} e^{i(q_x.X + q_y.Y)} \mathrm{d}X\mathrm{d}Y,$$

and can be expressed in polar coordinates as

$$S(\vec{q}) = \frac{\rho_{el}^2 r_e^2 L_x L_y}{q_z^2} \int e^{-\frac{q_z^2}{2} AR^{2h}} J_0(q_r R) R \, \mathrm{d}R, ,$$

with $q_r = \sqrt{q_x^2 + q_y^2}$ being the in-plane scattering wavevector and J_0 the zero order Bessel function. The above integral has analytical solutions for $h = 0.5$ and $h = 1$ and has to be calculated numerically in other cases.

For $h = 1$, $S(\vec{q}) = \dfrac{2\pi\rho^2 r_e^2 L_x L_y}{A q_z^4} e^{-q_r^2/2Aq_z^2}$,

and for $h = 0.5$, $S(\vec{q}) = \dfrac{A\pi\rho^2 r_e^2 L_x L_y}{\left(q_r^2 + \left(\frac{A}{2}\right)^2 q_z^4\right)^{3/2}}$.

The above expressions clearly show that for surfaces of this kind the scattering is purely *diffuse*. The case $h = 0.5$ is of particular interest since it corresponds to self-affine rough surfaces presenting a random walk character. Examples of such a surface have been recently encountered in Langmuir–Blodgett films of Cd-icosenoate and Cd-arachidate[27,28]. An example of diffuse scattering in such systems is presented in Figure 8.

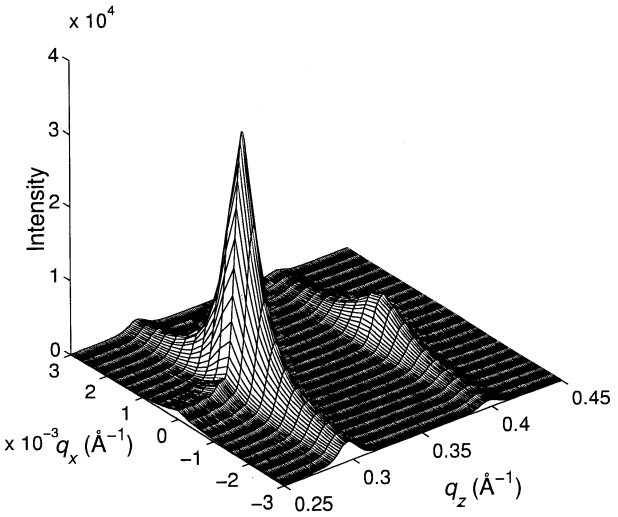

Figure 8. Diffuse scattering of 8-bilayes of Cd-tricosenoate LB film deposited on a silicon substrate.

4.4. *Rough surfaces with cut-off*

For rough surfaces presenting a cut-off length ξ, the development of $g(R)$ is no more possible and the scattering cross-section becomes

$$S(\vec{q}) = \frac{\rho_{el}^2 r_0^2 L_x L_y}{q_z^2} e^{-q_z^2\sigma^2} \iint_S e^{q_z^2 C(X,Y)} e^{i(q_x.X + q_y.Y)} \mathrm{d}X\mathrm{d}Y.$$

It is possible to separate this expression into the specular and the diffuse off-specular components by using the following method

$$e^{q_z^2 C(X,Y)} = 1 + (e^{q_z^2 C(X,Y)} - 1),$$

which yields

$$S(\vec{q}) = S_{spe}(\vec{q}) + S_{diff}(\vec{q}),$$

with

$$S_{spe}(\vec{q}) = \frac{\rho_{el}^2 r_e^2 L_x L_y}{q_z^2} e^{-q_z^2\sigma^2} \iint_S e^{-i(q_x.X + q_y.Y)} \mathrm{d}X\mathrm{d}Y$$

$$= \frac{4\pi^2 \rho_{el}^2 r_e^2 L_x L_y}{q_z^2} e^{-q_z^2\sigma^2} \delta q_x \delta q_y,$$

and

$$S_{diff}(\vec{q}) = \frac{\rho_{el}^2 r_e^2 L_x L_y}{q_z^2} e^{-q_z^2\sigma^2} \iint_S (e^{q_z^2 C(X,Y)} - 1) e^{i(q_x.X + q_y.Y)} \mathrm{d}X\mathrm{d}Y.$$

The specular part is similar to that of a flat surface except that it is reduced by the $e^{-q_z^2\sigma^2}$ roughness factor which is somewhat identical to a Debye–Waller factor.

The diffuse scattering part may be determined if one knows the functional form of the height–height correlation function. If a stretched exponential is chosen, the parameters h and ξ are obtained by fitting the above expression to the data. This approach has been used to analyse a variety of thin films and multilayers. A nice example concerning W/Si multilayers is presented in Salditt *et al.*[29]. A more precise treatment can be made within the distorted wave Born approximation (DWBA)[23,24]. This allows one to take into account the Yoneda wings which appear in the transverse scans[30]. The DWBA is extremely useful to explain strong effects of multiple scattering visible in thin films[31,32]. An example of how the diffuse scattering has been analysed in a Ge layer deposited on a Si(100) substrate[32] is presented in Figure 9. The DWBA has also been used to analyse liquid and polymer thin films[33].

So far in this paper, we have not yet considered the effect of the instrumental resolution on the reflectivity analysis. One must understand that this effect is of particular importance in the analysis of the diffuse scattering (for more details see refs 14 and 24). It is also important to realize that for very rough surfaces 'true specular re-

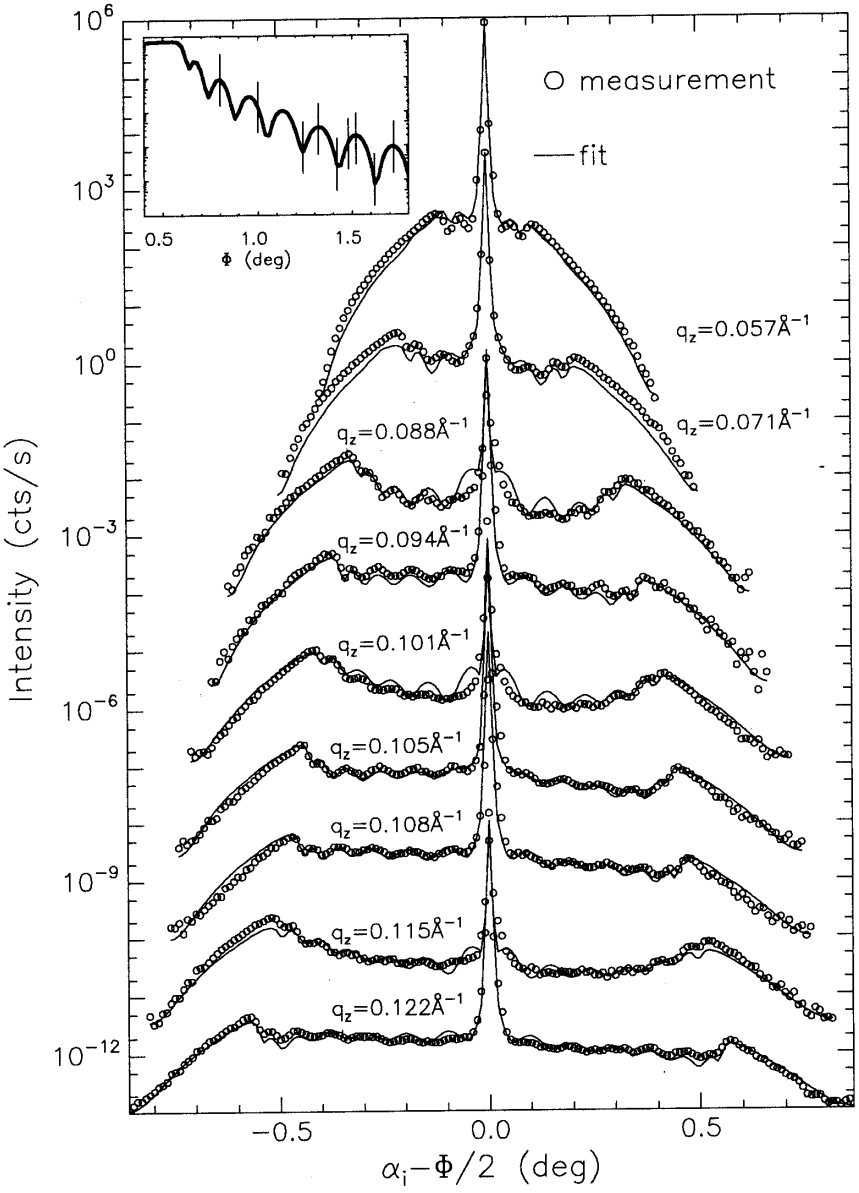

Figure 9. Diffuse scattering measured at different wave vector transfers q_z in a thin film of Ge deposited on Si (reproduced from permission of Schlomka *et al.*[32]). The inset shows the specular reflectivity and the lines the positions at which the transverse scans were made. The scans are presented as a function of the incident angle α_i. Apart from the presence of the Yoneda wings visible at both sides of the scans one can see some oscillations which are related to a dynamical effect.

flectivity' may not exist and that only diffuse scattering would be observed. For this reason any analysis of the specular reflectivity can only be valid under the condition that the diffuse scattering has been subtracted from the data.

5. Heterogeneous films

The total scattered intensity from a film can be calculated in the kinematical approximation (as mentioned in Section 3) as

$$I(q) = |\int \rho(r) e^{iq.r} \mathrm{d}V|^2.$$

For a heterogeneous thin film, where metal clusters are randomly distributed in the amorphous matrix, the above electron density can be written as[34]

$$\rho(r) = \left[\rho_{matrix} + \Delta\rho \sum_i \delta(r - r_i) \otimes S_{cluster}(r_i) \right] S_F(r),$$

where $\Delta\rho = \rho_{cluster} - \rho_{matrix}$, $S_{cluster}(r_i)$ is related to the shape and size of the ith cluster at a position r_i and $S_F(r)$ is related to the limited dimension of the film. We can assume that part of the incident beam is reflected by the film interfaces and part of it is scattered by metallic grains. Then the total scattered intensity can be written as the sum of two intensities arising separately from the matrix and the clusters (neglecting the matrix–cluster cross term) as

$$I(q_z) = I_{matrix} + I_{cluster},$$

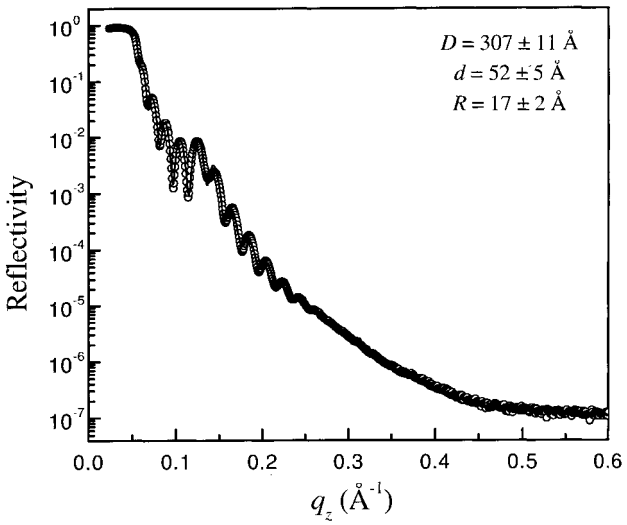

Figure 10. X-ray reflectivity of Pt-Al_2O_3 cermet thin film deposited on float glass. Best fit curve and the extracted parameters are also shown.

where I_{matrix} is due to the matrix and can be calculated considering a film of thickness D having homogeneous electron density as

$$I_{matrix} = \left| \frac{r_{0,1} + r_{1,2} e^{i2q_z D}}{1 + r_{0,1} r_{1,2} e^{i2q_z D}} \right|^2,$$

while $I_{cluster}$ can be calculated considering the shape, size and separation of the clusters. If we consider spherical clusters of radius R distributed in the matrix according to the cumulative disorder having average separation d then[34,35]

$$I_{cluster} \propto \frac{(\sin q_z R - q_z R \cos q_z R)^2}{(q_z R)^6} \times \frac{1 - e^{-2q_z^2 \sigma_d^2}}{1 - 2\cos(q_z d) e^{-q_z^2 \sigma_d^2} + e^{-2q_z^2 \sigma_d^2}},$$

where σ_d is the variance of d. In actual calculation one has to consider the variance of R as well, and take into account the effect of reduced dimension in the $I_{cluster}$ calculation. The typical reflectivity curve of Pt-Al_2O_3 cermet film deposited on float glass is shown in Figure 10. Extracted parameters and the best fit curve are shown in the figure. From these parameters and the diffuse scattering results one can predict the morphology of the nano-cermet thin films.

6. Conclusion

X-ray reflectometry is now widely used for the analysis of surfaces and interfaces. Its main advantage is that it allows one to determine the surface and interface roughness (when σ is typically less than 5 nm), the layer thickness (if typically less than 200 nm), EDP and the structural arrangement of complex architectures. Since measurements are made at small angles of incidence, it is not necessary for the analysed materials to be crystallized which is also an advantage of the technique over classical diffraction methods. However, it is also important to be cautious about this technique. Indeed due to phase loss, the uniqueness of the EDP which can be obtained from data analysis is never ensured. Some attempts which are now made to extract the density profile by direct inversion methods[36–38] represent a formidable challenge. The diffuse scattering which corresponds to the signal which is not specularly reflected gives additional information. In particular, one can learn from the diffuse scattering how the roughness of the interfaces is correlated both within one interface and from one interface to the next.

1. Stoev, K. N. and Sakurai, K., *Spectrochim. Acta, Part B*, 1999, **54**, 41.
2. Bowen, D. and Wormington, M., *Adv. X-Ray Anal.*, 1993, **36**, 171.
3. Van den Hoogendorf, W. and de Boer, D. K. G., *Surf. Interface Anal.*, 1994, **22**, 169.
4. Dietrich, S. and Haase, A., *Phys. Rep.*, 1995, **260**, 1.
5. Deutsch, M. and Ocko, B. M., *Encycl. Appl. Phys.*, 1998, **23**, 479.
6. Robinson, I. K. and Tweet, D. J., *Rep. Prog. Phys.*, 1992, **55**, 599.
7. Maoz, R., Cohen, S. R. and Sagiv, J., *Adv. Mater.*, 1999, **11**, 55.
8. Compton, A. H., *Philos. Mag.*, 1923, **45**, 112.
9. Croce, P. and Névot, L., *Rev. Phys. Appl.*, 1976, **11**, 113–125; Névot, L. and Croce, P., *Rev. Phys. Appl.*, 1980, **15**, 761.
10. de Boer, D. K. G., *Phys. Rev. B*, 1994, **49**, 5817.
11. Abeles, F., *Ann. Phys.*, 1950, **5**, 596.
12. Parrat, L. G., *Phys. Rev.*, 1954, **95**, 359.
13. Born, M. and Wolf, E., *Principles of Optics*, Pergamon, London, 1980, 6th edn.
14. Gibaud, A., Vignaud, G. and Sinha, S. K., *Acta Crystallogr. A*, 1993, **49**, 642.
15. Gibaud, A., Mc Morrow, D. and Swaddling, P. P., *Phys. Condens Matter*, 1995, **7**, 2645.
16. Vidal, B. and Vincent, P., *Appl. Optics*, 1984, **23**, 1794.
17. Stearns, D. G., *J. Appl. Phys.*, 1992, **71**, 4286.
18. Hamley, I. W. and Pedersen, J. S., *J. Appl. Crystallogr.*, 1994, **27**, 29.
19. Als-Nielsen, J., *Z. Phys. B*, 1985, **61**, 411.
20. Wu, X. Z., Sirota, E. B., Sinha, S. K., Ocko B. M. and Deutsch, M., *Phys. Rev. Lett.*, 1993, **70**, 958.
21. Vignaud, G., Gibaud, A., Grübel, G., Joly, S., Ausserré, D. Legrand, J. F. and Gallot, Y., *Physica B*, 1998, **248**, 250.
22. Bridou, F. and Pardo, B., *J. Phys. III, France*, 1994, **4**, 1523.
23. Sinha, S. K., Sirota, E. B., Garoff, S. and Stanley, H. B., *Phys. Rev. B*, 1988, **38**, 2297.
24. Daillant, J. and Bélorgey, O., *J. Chem. Phys.*, 1992, **97**, 5824.
25. Basu, J. K. and Sanyal, M. K., *Phys. Rev. Lett.*, 1997, **79**, 4617.
26. Sanyal, M. K., Sinha, S. K., Huang, K. G. and Ocko, B. M., *Phys. Rev. Lett.*, 1991, **66**, 628.
27. Gibaud, A., Cowlam, N., Vignaud, G. and Richardson, T., *Phys. Rev. Lett.*, 1995, **74**, 2305.
28. Basu, J. K., Hazra, S. and Sanyal, M. K., *Phys. Rev. Lett.*, 1999, **82**, 4675.
29. Salditt, T., Lott, D., Metzger, T. H., Peisl, J., Vignaud, G., Hogho, P., Schärpf, O., Hinze, P. and Lauer, R., *Phys. Rev. B*, 1996, **54**, 5860.
30. Yoneda, Y., *Phys. Rev.*, 1963, **113**, 2010.
31. Holy, V., Kubena, J., Ohidal, I., Lischka, K. and Plotz, W., *Phys. Rev. B*, 1993, **47**, 15896.
32. Schlomka, J. P., Tolan, M., Schwalowsky, L., Seeck, O. H., Stettner, J. and Press, W., *Phys. Rev. B*, 1995, **51**, 2311.
33. Daillant, J., Quinn, K., Gourier, C. and Rieutord, F., *J. Chem. Soc., Faraday Trans.*, 1996, **92**, 505.
34. Maaza, M., Gibaud, A., Sella, C., Pardo, B., Dunsteter, F., Corno, J., Bridou, F., Vignaud, G., Désert, A. and Menelle, A., *Eur. Phys. J. B*, 1999, **7**, 339.
35. Vainshtein, B. K., in *Diffraction of X-rays by Chain Molecules*, Elsevier, Amsterdam, 1966.
36. Sanyal, M. K., Hazra, S., Basu, J. K. and Datta, A., *Phys. Rev. B*, 1998, **58**, R4258.
37. Majkrak, C. F. and Berk, N. F., *Phys. Rev. B*, 1995, **52**, 10827.
38. Sinha, S. K., Sanyal, M. K., Huang, K. G., Gibaud, A., Rafailovich, M., Sokolov, J., Zhao, X. and Zhao, W., in *Surface X-ray and Neutron Scattering* (eds Zable, H. and Robinson, I. K.), Springer-Verlag, Berlin, 1992, p. 85.